Scaling relation between anomalous Nernst and Hall effect in $[Pt/Co]_n$ multilayers

C. Fang, C. H. Wan,* Z. H. Yuan, L. Huang, X. Zhang, H. Wu, Q. T. Zhang, and X. F. Han†
Institute of Physics, Chinese Academy of Sciences, Beijing 100190, China
(Received 16 December 2015; published 23 February 2016)

The anomalous Nernst coefficient, anomalous Hall angle, and Seebeck coefficient have been measured in the same series of $[Pt/Co]_n$ superlattices in which spin-orbit coupling is dominated by interfaces. With an increase in the number of interfaces from 1 to 15, the anomalous Nernst coefficient and anomalous Hall angle simultaneously increase, by 350% and 430%, respectively. Furthermore, they even scale linearly with each other, while the Seebeck coefficient and magnetization of the superlattices vary a little. Based on the linear scaling relation, a physical scenario behind the anomalous Nernst effect, as well as a formula relating the Nernst coefficient, the Hall angle, and the Seebeck coefficient, is proposed. The work not only demonstrates an effective way to enhance the anomalous Nernst effect in ferromagnetic conductors but also can bring about deeper insight into the anomalous Nernst effect.

DOI: 10.1103/PhysRevB.93.054420

I. INTRODUCTION

Spin caloritronics, focusing on the interplay of spin current or spin accumulation with a thermal gradient, has emerged rapidly as an important spintronics branch due to its potential prospects in waste heat recycling in today's microelectronics since the discovery of the spin Seebeck effect (SSE) [1–12], spin-dependent Seebeck effect (SDSE) in magnetic tunnel junctions [13–15], SDSE in giant magnetoresistance devices [16–18], and spin-dependent Peltier effect [19,20]. Studies on the anomalous Nernst effect (ANE) in which a temperature gradient $\partial T/\partial x$ can produce an electric field $\partial V_N/\partial y$ in a ferromagnetic conductor with magnetization along the z axis have been revived as well because of its ability to generate electricity from thermal energy. The V_N is the so-called anomalous Nernst voltage, which, though discovered more than one century ago, is not thoroughly understood [21].

Recently, Ramos *et al.* [21] and Pu *et al.* [22] researched the temperature (T) dependence of V_N, the Seebeck coefficient (S), and the Hall angle (θ_H) in thick Fe_3O_4 and $Ga_{1-x}Mn_xAs$ films, respectively, and found that V_N and S both satisfy the Mott relation. Hasegawa *et al.* researched the T dependence of V_N, S, and the anisotropy energy in some perpendicular systems such as FePt, FePd, $D0_{22}$ Mn_2Ga, $L1_0$ MnGa, and Co/Ni thick films [23]. Their results show a positive correlation between V_N and the anisotropy energy. Uchida *et al.* [24] researched V_N in $[Fe/Pt]_n$, $[Au/Fe]_n$, and $[Cu/Fe]_n$ stacks and found an enhancement of the ANE in stacks with heavier elements. These pioneering works have indicated a strong correlation among V_N, S, and the spin-orbit coupling (SOC) strength. However, an experimental work directly relating V_N, S, and θ_H in the same material system with variable SOC strengths is still lacking. A clear physical picture behind the ANE is still to be revealed.

In this research, we have systematically measured the V_N, S, and θ_H of $[Pt/Co]_n$ superlattices in which the SOC strength can be monotonically modulated by the number of interfaces. A positive correlation, especially, a linear scaling relation between V_N and θ_H, has been clearly observed with a relatively stable S and saturated magnetization (M_0). Based on this relation, we propose a physical picture behind the ANE, which may lead to a more comprehensive understanding of this long-mysterious effect.

II. SAMPLES AND EXPERIMENTS

$[Co(t\ \text{nm})/Pt(t\ \text{nm})]_n (n = 1\text{–}8,\ t = 12/n)$ stacks were deposited on Si(500 μm)/SiO_2(500 nm) substrates with a base pressure of 1.0×10^{-6} Pa at room temperature with a TMR R&D Sputtering System (ULVAC). The number of Co/Pt interfaces increases as $(2n - 1)$, while their total thickness is kept at 12 nm to maintain the transport properties of the bulk region as stable as possible. A magnetic field of 200 Oe around the sample holder is equipped in the sputtering system to induce an easy axis. Co (12 nm), Pt (12 nm), and X (20 nm)/Pt (2 nm) ($X = Ni_{80}Fe_{20}$, $Co_{40}Fe_{40}B_{20}$, Co) films were fabricated for comparison.

Films were then patterned via one-step ultraviolet lithography and the following argon etching process. For anomalous Hall effect (AHE) and resistivity measurement, films were patterned as a Hall bar as shown in Fig. 1(a) with the easy axis along the x axis. In this case, current (I) is applied between pad G and pad H, and voltmeters pick up V_{PQ} and V_{PL} for measuring $R_{xx} = V_{PQ}/I$ and $R_{xy} = V_{PL}/I$, respectively. For ANE measurement, films were patterned as shown in Fig. 1(b) with points E and F along the easy axis. During ANE measurement, heating current (I) is applied between pad A and pad B, generating a temperature gradient in the transverse direction along the x axis ($\partial T/\partial x$). The magnitude of $\partial T/\partial x$ is controlled by the heating power ω ($\omega = I^2 R_{AB}$, with R_{AB} being the resistance between pad A and pad B). In the x direction, no net current flows between point E and pad F because the circuit for measuring ANE was isolated from the heating bar by a fixed distance D of 7 μm. Pads C and D are used to detect Nernst voltages. It is noteworthy that the anomalous Nernst voltage measured in this setup can be free of contamination from the SSE and planary Nernst effect (PNE) induced by $\partial T/\partial x$ or $\partial T/\partial z$ (if it exists) if magnetization is fully saturated along the $\pm z$ axis. The absence of the SSE is due to the collinear alignment of spin polarization of the spin current driven by the SSE (parallel to magnetization) with the

*wancaihua@iphy.ac.cn
†xfhan@iphy.ac.cn

 ©2016 American Physical Society

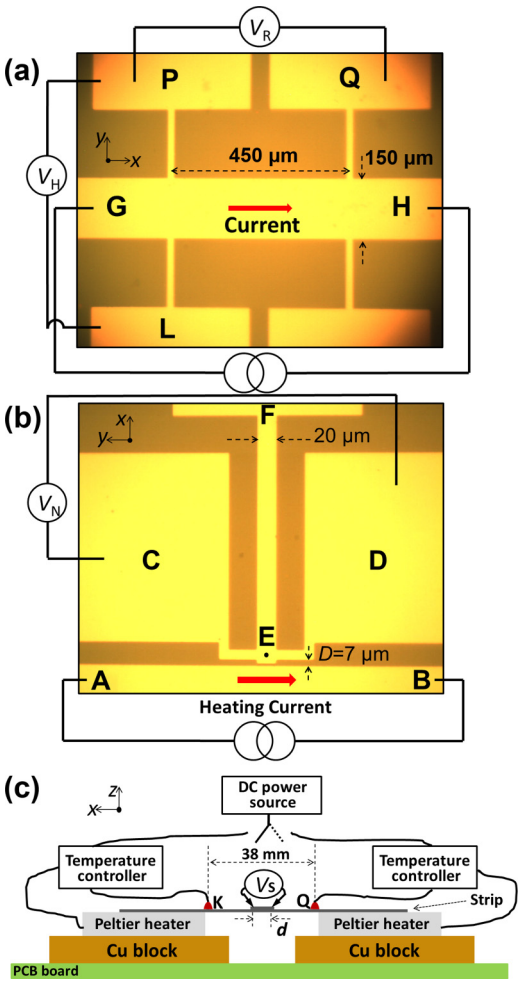

FIG. 1. Patterns for measuring (a) the resistance and Hall resistance and (b) the anomalous Nernst effect. Point E and pad F are along the easy axis and also along the x axis. (c) Schematic of the experimental setup for measuring the Seebeck coefficient of a thin film. Tungsten probes with a spacing of d are used to pick up the Seebeck voltage. The temperature gradient between point K and point Q in a silicon strip, after the geometry factor ξ is taken into account, is used to estimate the counterpart in a sample on the top of the strip. A thin layer of thermal grease has to be used between the sample and the strip to improve the interfacial thermal conductivity and obtain a high signal-to-noise ratio of the Seebeck voltage.

film normal. The absence of the PNE is due to the fact that the PNE is similar to the planary Hall effect and is proportional to $\cos\theta \sin\theta$, with θ being the angle between magnetization and temperature gradient. Dimensions of different measurement setups are also shown in Figs. 1(a) and 1(b). H_z was provided by a Physical Property Measurement System (PPMS-9T; Quantum Design). The Keithley 2400 and Keithley 2182 were applied to source samples and measure voltages, respectively.

It is also worth mentioning that the increase in resistivity of the superlattices would lead to a decrease in their thermal conductivity according to the Wiedemann-Franz law [25] by about 1 time. Nevertheless, the decrease in thermal conductivity of a thin film from 30 W/(m · K) [25] to even 1 W/(m · K) would lead to an increase of only about 10% in $\partial T/\partial x$ around point E according to finite-element modeling because the thermal conductance of the substrate is several orders of magnitude higher than that of the thin film, and the heat flow as well as the temperature distribution is thus determined by the substrate instead of the film. Here the thermal conductivity of SiO_2 and Si is selected to be 1.4 W/(m · K) and 148 W/(m · K) [26] in the finite-element modeling. Evidently, our Nernst measurement setup can well separate electrotransport in the film and heat transport in the substrate.

Seebeck coefficients of samples were measured in a homemade facility equipped with two Peltier heaters, two temperature controllers, and a three-dimensional magnet (±300 Oe in three directions realized by Helmholtz coils) [Fig. 1(c)]. Two copper blocks were fixed on a PCB board to aid heat dissipation. The Peltier heaters were placed on top of the copper blocks with a spacing of 40 mm. A silicon strip of 70 mm × 12 mm × 500 μm connected the top sides of the two heaters. Then a temperature gradient was built along the strip after one heater was turned on. To estimate the temperature gradient along the strip, we placed two temperature sensors at points K and Q on the top of the strip, with their spacing L being 38 mm. The sensors are connected to the temperature controllers for PID control. Samples with a width of 5 mm and a length l of 8.5 mm were placed on the center of the strip to feel the temperature gradient. Either the easy or the hard axis of the samples was parallel to the x axis. There was no observable difference between these two cases. After about 5 min of stabilization, the Seebeck voltage V_S was picked up by the Keithley 2182 via two tungsten probes whose absolute Seebeck coefficient was about 2.5 μV/K at 300 K. The distance d between the two probes was about 8 mm. Thus a temperature difference, $\Delta T = \xi \Delta T_{KQ} d/L$, was estimated to be built between the probes along a sample. Here ξ, a geometry factor, had to be introduced due to the influence of the sample on the local temperature distribution, and it was about 0.56 determined by finite-element calculation with real dimensions. In order to improve the interfacial thermal conductivity, a thin layer of thermal grease was used between the heaters and the strip and also between the strip and the substrate of samples. The geometry factor ξ is insensitive to the thickness of the thermal grease as long as the thickness of the thermal grease is much smaller than that of the silicon strip.

III. ANOMALOUS HALL EFFECT

Figure 2(a) shows the H_z dependence of the Hall resistivity (ρ_{xy}) of the samples (SPn; n = 1–8) at 300 K. The ρ_{xy} and resistivity ρ_{xx} both increase monotonically with $(2n-1)$ [Fig. 2(a); inset], hinting at a remarkable effect of interface scattering. A similar phenomenon was reported by Canedy *et al.* [27] and Zhao *et al.* [28]. As $n \leqslant 5$, $\theta_H \equiv \rho_{xy}/\rho_{xx} = 0.0049 + 0.0027(2n-1)$ [Fig. 2(b)]. It is reasonable that the intercept 0.0049 is just about half the θ_H of pure Co, which is 0.011, considering that $\sigma_{Pt}/\sigma_{Co} \approx 1.1$. This part results from bulk Co. The rest, linearly depending on $(2n-1)$, is attributed to interface scattering. It is noteworthy that the interfacial part contributes more than the bulk part to θ_H as $n \geqslant 2$. The scaling law $\rho_{xy} \propto \rho_{xx}^{\beta}$ is measured by varying T [Fig. 2(c)]. If an intrinsic or side-jump mechanism dominates the AHE, β is close to 2. Otherwise, it is close to 1 if skew scattering dominates [29]. Here the β of Co

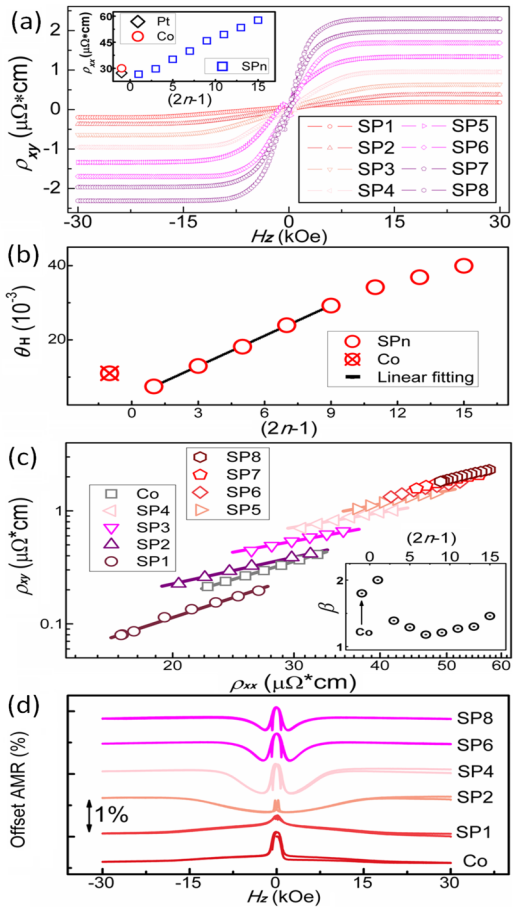

FIG. 2. (a) H_z dependence of ρ_{xy} of SPn at 300 K. Inset: Dependence of ρ_{xx} on $(2n-1)$ at 300 K. (b) Dependence of θ_H at 300 K on $(2n-1)$ and its linear fitting as $n \leqslant 5$. (c) Scaling law between ρ_{xy} and ρ_{xx} with varying T. Inset: Scaling exponent β. (d) H_z dependence of the anisotropic magnetoresistance of Co and some superlattices.

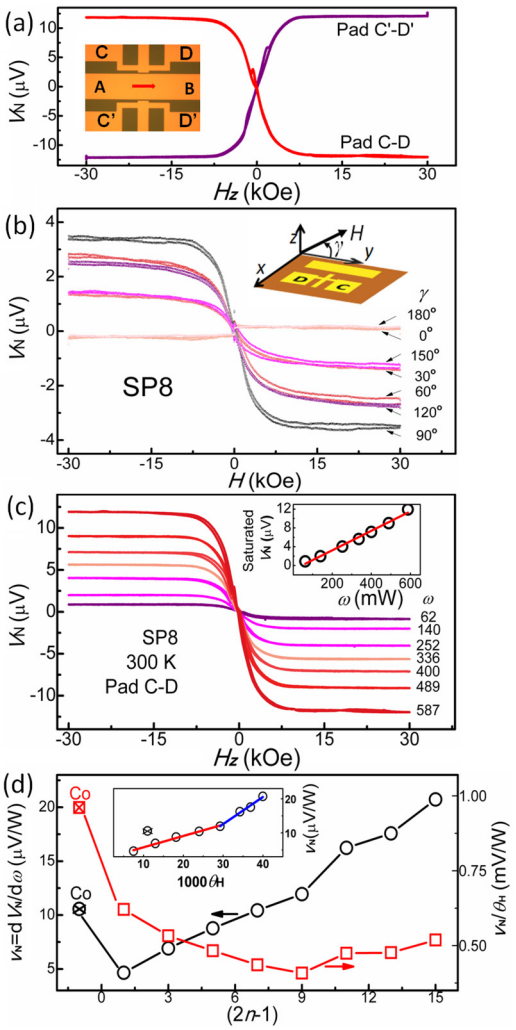

FIG. 3. (a) Field dependence of the V_N of SP8 under opposite $\partial T/\partial x$ and $\omega = 587$ mW. Inset: Positions of corresponding pads. (b) Field dependence of the V_N of SP8 under different γ at $\omega = 250$ mW. Inset: Definition of the angle γ. (c) Field dependence of the V_N of SP8 under elevated powers. Inset: Linear dependence of saturated V_N on ω. The solid red line shows the linear fitting result. (d) Dependence of $\nu_N = \mathrm{d}V_N/\mathrm{d}\omega$ (left axis) and ν_N/θ_H (right axis) on the number of interfaces. Inset: Scaling relation between ν_N and θ_H of the superlattices. Solid red and blue lines show linear fitting results as $n \leqslant 5$ and $n \geqslant 5$, respectively.

and SP1 is 1.8 and 2, respectively, while the β of the rest samples is reduced to 1.3 ± 0.1 [Fig. 2(c); inset]. The sudden drop in β at $n = 2$ also indicates the dominating role of interface skew scattering as $n \geqslant 2$. We have also measured the anisotropic magnetoresistance (AMR) of Co and some superlattices [Fig. 2(d)] as H is applied along the z axis. They are all within 1%. The H_z dependence of the AMR seems to be composed of two parts: one within 3 kOe and the other saturated within about 15 kOe. The first one shows $\rho_\parallel \geqslant \rho_\perp$ always, which is ordinary and unchanged in the superlattices. $\rho_\parallel$ and $\rho_\perp$ is the resistivity with magnetization parallel and normal to the current density, respectively. The second one shows $\rho_\parallel \geqslant \rho_\perp$ for Co and SP1. However, $\rho_\parallel \leqslant \rho_\perp$ for the other superlattices. A similar AMR where $\rho_\parallel \leqslant \rho_\perp$ has also been reported at the Au/YIG interface [4]. Though it is abnormal, the origin of this AMR is beyond the scope of this article and will be discussed elsewhere.

IV. ANOMALOUS NERNST EFFECT

We also measured the ANE of different samples. In our Nernst measurement setup, though the heating bar is also made of the superlattices, the AMR of the heating bar will only introduce uncertainly of the Nernst voltage within 1%. The anomalous Nernst voltage V_N evolves with H_z in a very similar way as ρ_{xy} does. As a typical feature of the ANE, the sign of V_N is reversed with reversing $\partial T/\partial x$ [Fig. 3(a) and its inset]. As H is rotated from out-of-plane to in-plane [γ, defined in the inset to Fig. 3(b), becomes 0° or 180°], V_N becomes gradually negligible [Fig. 3(b)]. This observation also supports a physical picture of the ANE which requires orthogonality among M, ∇T, and ∇V_N. The ordinary Nernst effect which depends linearly on H_z is negligible, compared with the ANE [Fig. 3(a)]. Besides, a small planary Nernst effect only appears around zero fields, while it disappears after saturation of M. V_N increases linearly with the heating power ω as expected

[Fig. 3(c) and its inset] and $\nu_N \equiv dV_N/d\omega$ is thus defined to indirectly characterize the ANE coefficient (η) in this study. Figure 3(d) shows that the ν_N of SP1 is about half the ν_N of pure Co due to the shielding effect of Pt. Besides, similarly to θ_H, the ν_N of the superlattices also monotonically increases with $(2n-1)$, by 350% from $n=1$ to $n=8$, indicating that interfacial contact with Pt is a highly effective way to enhance the ANE in superlattice systems. Meanwhile, θ_H increases by 430% from $n=1$ to $n=8$. The coefficient of correlation defined as $\sum_{i=1}^{8}(\nu_{\rm Ni}\theta_{\rm Hi})/[(\sum_{i=1}^{8}\nu_{\rm Ni}^2)^{1/2}(\sum_{i=1}^{8}\theta_{\rm Hi}^2)^{1/2}]$ reaches 0.997. More importantly, ν_N linearly scales with θ_H as $n \leqslant 5$ and $n \geqslant 5$ with a slope $d\nu_N/d\theta_H$ of (0.33 ± 0.02) mV/W and (0.80 ± 0.06) mV/W [Fig. 3(d); inset], respectively. The ratio of ν_N/θ_H was also checked [Fig. 3(d); right]. The ν_N/θ_H in Co is 0.96 mV/W, while the average ν_N/θ_H over the eight superlattices is (0.49 ± 0.07) mV/W. The positive correlation and, especially, the linear relation between ν_N and θ_H observed in the same material system strongly imply that the same microscopic origin is responsible for the ANE and AHE, which is discussed below.

V. SCALING RELATION BETWEEN THE AHE AND THE ANE

The positive correlation between η and SOC strength in different perpendicular ferromagnetic materials was also suggested recently in Ref. [23]. Here the linear scaling relation between η and θ_H observed in the same series of $[Co/Pt)]_n$ stacks further indicates a strong correlation between them. In order to understand this relation, let us turn to the linear response theory below as proposed in Ref. [2]. For a ferromagnetic conductor, according to this theory, the density of the charge current J_c, spin current J_s, and heat flow Q are driven by the gradient of the electrochemical potential $\nabla\mu_c$, spin potential $\nabla\mu_s$, and temperature ∇T, respectively, via Eq. (1):

$$\begin{bmatrix} J_c \\ J_s \\ Q \end{bmatrix} = \sigma \begin{bmatrix} 1 & P & ST \\ P & 1 & P_T ST \\ ST & P_T ST & \kappa T/\sigma \end{bmatrix} \begin{bmatrix} \nabla\mu_c/e \\ \nabla\mu_s/2e \\ -\nabla T/T \end{bmatrix} \quad (1)$$

Here $J_{c/s} = J_\uparrow \pm J_\downarrow$. $J_\uparrow$ and $J_\downarrow$ are the current density in spin-up and spin-down channels. $\mu_c = (\mu_\uparrow + \mu_\downarrow)/2$ and $\mu_s = (\mu_\uparrow - \mu_\downarrow)$, with $\mu_\uparrow$ and $\mu_\downarrow$ being the electrochemical potential of spin-up and spin-down electrons. S, σ, and κ are the Seebeck coefficient, conductivity, and thermal conductivity, respectively. σS is the thermoelectric conductivity. $S = (S_\uparrow\sigma_\uparrow + S_\downarrow\sigma_\downarrow)/(\sigma_\uparrow + \sigma_\downarrow)$ and $\sigma = \sigma_\uparrow + \sigma_\downarrow$. $P \equiv (\sigma_\uparrow - \sigma_\downarrow)/(\sigma_\uparrow + \sigma_\downarrow)$. $\sigma_{\uparrow/\downarrow}$ and $S_{\uparrow/\downarrow}$ are the spin-dependent conductivity and Seebeck coefficient, respectively. $P_T \equiv [\partial(P\sigma)/\partial\epsilon|_{\epsilon_F}]/[\partial\sigma/\partial\epsilon|_{\epsilon_F}]$. Actually, P_T can be reduced as $(\sigma_\uparrow S_\uparrow - \sigma_\downarrow S_\downarrow)/(\sigma_\uparrow S_\uparrow + \sigma_\downarrow S_\downarrow)$ after the Mott relation $\sigma_i S_i = \frac{\pi^2}{3}(\frac{k}{e})(kT)\frac{d\sigma_i}{d\epsilon}$ is taken into account. P_T can thus be deemed the spin polarization of the thermoelectric conductivity. In the case of an open circuit, $\nabla\mu_c = eS\nabla T$. Then $J_s = (P - P_T)\sigma S\nabla T$, which is exactly equivalent to the J_s expression in Ref. [16]. This equation implies that ∇T can produce a pure spin current in a ferromagnetic conductor if $P \neq P_T$ or $S_\uparrow \neq S_\downarrow$. Further, we propose here that conversion of this pure spin current into a transverse charge current via the inverse spin Hall effect (ISHE) in a ferromagnetic conductor finally results in an anomalous Nernst voltage. Actually, the ISHE in a ferromagnetic conductor has been observed in Refs. [8] and [30]. In the following, we phenomenologically discuss how a spin-polarized charge current and a pure spin current are transformed into a transverse charge current through the ISHE in the AHE and ANE, respectively, and then acquire the final relation among the anomalous Nernst coefficient, Seebeck coefficient, and anomalous Hall angle.

In the AHE, the charge current density J applied to the x axis can be decomposed into two parts: $J(1+P)/2$ for spin-up and $J(1-P)/2$ for spin-down channels. Without any loss of generality, we further suppose that electrons with opposite spins can (but do not necessarily) have different spin Hall angles $\theta_{\uparrow/\downarrow}$. $P_\theta \equiv (\theta_\uparrow - \theta_\downarrow)/(\theta_\uparrow + \theta_\downarrow)$ and let the average spin Hall angle $\theta_s \equiv (\theta_\uparrow + \theta_\downarrow)/2$. Thus a transverse current along the y axis $J_c = \theta_\uparrow J(1+P)/2 - \theta_\downarrow J(1-P)/2 = \theta_s J(P + P_\theta)$ is generated via the ISHE. The anomalous Hall angle θ_H equal to J_c/J is thus $\theta_s(P + P_\theta)$.

In the SDSE, the pure spin current density J_s generated by ∇T can also be decomposed into two parts: $J_s/2$ for each spin channel. These two spin currents, with opposite spin polarization directions and opposite moving directions, can be deflected into the same transverse direction and cooperatively contribute to a charge current of $J_c = \theta_\uparrow J_s/2 + \theta_\downarrow J_s/2 = \theta_s J_s$. Recalling the relation between J_s and ∇T as well as the relation between θ_s and θ_H, one can easily obtain $\nabla V_N = (P - P_T)/(P + P_\theta)\theta_H S\nabla T$. The anomalous Nernst coefficient η defined as $\nabla V_N/(\mu_0 M_0 \nabla T)$ can then be expressed via Eq. (2), which clearly shows a linear dependence of η on θ_H and S with coefficient $(P - P_T)/(P + P_\theta)/(\mu_0 M_0)$ depending on the spin polarization of the conductivity, thermoelectric conductivity, and spin Hall angle. Here μ_0 and M_0 are the permeability of vacuum and saturated magnetization, respectively. A similar linear relation between η and θ_H has been suggested in nonmagnetic materials [31]. In these systems, $\theta_H \approx \mu B$ and μ is the mobility. Thus η linearly depends on μ. However, such a relation has not been proposed in ferromagnetic materials before:

$$\eta = (P - P_T)/(P + P_\theta)\theta_H S/(\mu_0 M_0). \quad (2)$$

In the recent Ref. [21], $\theta_H S$ was found to contribute partially to $\mu_0 M_0 \eta$. Nevertheless, the meaning of the extra part $(\mu_0 M_0 \eta - \theta_H S)$ is unknown. Here we can see from Eq. (2) that $(\mu_0 M_0 \eta - \theta_H S)/(\theta_H S) = -(P + P_T)/(P + P_\theta)$ relates closely to some basic material-sensitive parameters.

Equation (2) can also be derived from Eq. (A1) in Ref. [21], where $S_{xy} \equiv E_y/\nabla_x T = \rho\alpha_{xy} - S\tan\theta_H$. Here α and α_{xy} are the diagonal and nondiagonal elements of the thermoelectric conductivity tensor, respectively. $\alpha = \sigma S$. We define another angle (the thermoelectric angle $\delta_{\rm TE}$) as $\tan(\delta_{\rm TE}) \equiv \alpha_{xy}/\alpha$ to aid analysis. Normally, θ_H and $\delta_{\rm TE}$ are both much smaller than 1. Thus $S_{xy} = \rho\alpha_{xy} - S\tan\theta_H = (\delta_{\rm TE} - \theta_H)S$. Besides S, S_{xy} is also proportional to the difference between the thermoelectric angle and the anomalous Hall angle. $\theta_H = \theta_s(P + P_\theta)$. Similarly, $\delta_{\rm TE} = \theta_s(P_T + P_\theta)$ as shown below. ∇T drives two currents with opposite spin polarization via $J_{\uparrow/\downarrow} = \alpha_{\uparrow/\downarrow}\nabla T$. Here only thermoelectrotransport is considered. $\alpha_{\uparrow/\downarrow} = \sigma_{\uparrow/\downarrow}S_{\uparrow/\downarrow}$. These two currents will be deflected towards opposite transverse directions by the SOC

effect via $\theta_{\uparrow/\downarrow} J_{\uparrow/\downarrow} = \theta_{\uparrow/\downarrow}\alpha_{\uparrow/\downarrow}\nabla T$. The deflected transverse currents contribute to a net charge current of $J_{\text{net,transverse}} = \theta_\uparrow J_\uparrow - \theta_\downarrow J_\downarrow = \theta_\uparrow\alpha_\uparrow\nabla T - \theta_\downarrow\alpha_\downarrow\nabla T = \alpha_{xy}\nabla T$. The equation $J_{\text{net,transverse}} = \alpha_{xy}\nabla T$ is used according to the definition of α_{xy}, which says that the transverse charge current is driven by the ∇T. Thus $\delta_{\text{TE}} = (P_T + P_\theta)\theta_s$. Here we have used the relations $\theta_{\uparrow/\downarrow} = (1 \pm P_\theta)\theta_s$, $\alpha = \alpha_\uparrow + \alpha_\downarrow$, and $P_T = (\alpha_\uparrow - \alpha_\downarrow)/(\alpha_\uparrow + \alpha_\downarrow)$. Therefore $S_{xy} = (\delta_{\text{TE}} - \theta_H)S = -(P - P_T)/(P + P_\theta)\theta_H S$, which shares the same form as Eq. (2) except for the minus sign. Equation (2) can thus also be reproduced from Eq. (A1) in Ref. [21] under the assumption of an ISHE in ferromagnetic layers. This assumption has also been applied in recent theoretical literature [32] and experimentally demonstrated in many experiments [8,30].

Though built in a single-layer system, this phenomenological model can also be cautiously generalized into multilayer systems if the parameters in the model, such as ρ, θ_H, and S_{xy} of a single layer, are replaced with the corresponding effective parameters of the multilayers. Some specialty of the multilayer system, such as interfacial scattering, determines the values of those effective parameters and can thus be implicitly reflected in the model.

VI. MAGNETIZATIONS AND SEEBECK COEFFICIENTS

In order to check Eq. (2), we have also measured the saturated magnetization M_0 [Figs. 4(a) and 4(b)] and Seebeck coefficient of the superlattices [Figs. 4(c) and 4(d)] in the setup shown in Fig. 1(c). First, the dependence of M_0 on $(2n-1)$ is not strong. M_0 averaged over all samples is about 1370 emu/cc (only 12 nm Co is taken into account in estimating M_0). There appears to be a trend, though not obvious, that M_0 increases slowly as $n \geqslant 5$. This increase in M_0 may come from the interfacial proximity effect of Pt, which is common in Co/Pt multilayer systems [33,34].

At the beginning of Seebeck coefficient measurement, we applied ±300 Oe in all three directions to check the field dependence of the Seebeck voltage V_S. According to the M-H curve [from SP8 as shown in Fig. 4(a)], ±300 Oe is large enough to saturate magnetization in the x and y directions. However, no observable field dependence of V_S was found, indicating the absence of the ANE and SSE driven by $\partial T/\partial z$ and also the absence of the PNE driven by $\partial T/\partial x$ in the V_S signal. We then checked the dependence of V_S on ΔT and found $V_S = (S - S_W)\Delta T$ as expected [Fig. 4(c)], where S_W (2.5 μV/K) and S are the absolute Seebeck coefficients of the tungsten probes and samples, respectively. The S values of the superlattices as well as those of Co, Pt, NiFe, and CoFeB are shown in Fig. 4(d). S_{Co} and S_{NiFe} are both negative in sign and their magnitudes are also close to their literature values [17,35], while S_{Pt} is close to 0. S_n is located between S_{Co} and S_{Pt}. The average S_n over all the superlattices is (-10 ± 4) μV/K, similar to $(\sigma_{\text{Co}}S_{\text{Co}} + \sigma_{\text{Pt}}S_{\text{Pt}})/(\sigma_{\text{Co}} + \sigma_{\text{Pt}})$. According to Eq. (2), the relatively small variation in S_n and M_0 cannot explain the 350% increase in ν_N, which reflects from the other side a strong correlation between ν_N and θ_H in our superlattices. Besides, the average ratio ν_N/θ_H and the average S_n both decrease by half from Co to superlattices, which persuades us to attribute the decrease in ν_N/θ_H to the decrease in Seebeck coefficient according to Eq. (2). The increase in $\mathrm{d}\nu_N/\mathrm{d}\theta_H$ as $n \geqslant 5$ may be ascribed to the small increase in M_0 as well as in $|S_n|$ as $n \geqslant 5$.

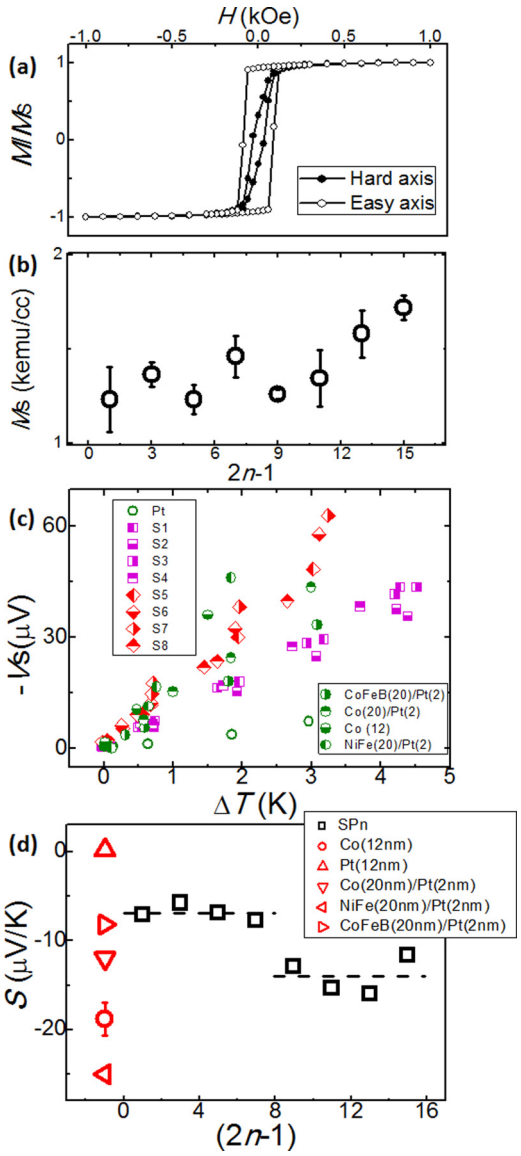

FIG. 4. (a) M-H curves of SP8 with H along the in-plane easy and hard axes. (b) Dependence of the M_0 of the superlattices on $(2n-1)$. (c) Dependence of the Seebeck voltage on the temperature difference. (d) Seebeck coefficient of the superlattices as well as some reference samples.

VII. TESTIFYING OF EQ. (2) IN COMMON FERROMAGNETS

We have also measured the Seebeck coefficients, AHE [Fig. 5(a)], and ANE [Figs. 5(b)–5(d)] of X(20 nm)/Pt(2 nm) with X = Co, CoFeB, and NiFe. Their θ_H values are 0.011, 0.048, and 0.0032, respectively. Their ν_N values are 7.3, 22, and 11 μV/W, respectively. Their Seebeck coefficients $|S|$ are 12, 8.2, and 25 μV/K, respectively. The value $|\nu_N/(\theta_H S)|$ obtained in Co(20 nm)/Pt(2 nm) is 55 K/W, close to the 48 K/W obtained in the pure Co(12 nm) sample. It is interesting to look deeply into the data on NiFe and CoFeB. Though

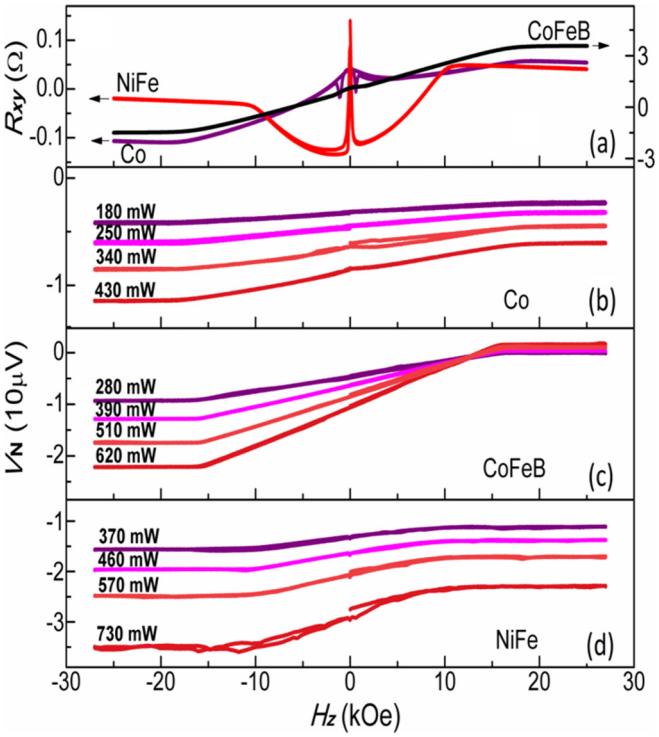

FIG. 5. (a) H_z dependence of R_{xy} and (b, c, d) H_z dependence of V_N of X (20 nm; Co, $Co_{40}Fe_{40}B_{20}$, and $Ni_{80}Fe_{20}$)/Pt(2 nm) at an elevated heating power ω, respectively.

$\theta_{H,CoFeB} = 15\theta_{H,NiFe}$, $S_{CoFeB} \approx 1/3 S_{NiFe}$. Thus $\nu_{N,CoFeB}$ does not differ from $\nu_{N,NiFe}$ by magnitudes. $\nu_{N,CoFeB}$ is only twice $\nu_{N,NiFe}$. These data in the different materials, we think, also qualitatively satisfy Eq. (2).

It deserves special attention that θ_H or the strength of SOC is mainly dominated by interfaces between Pt and Co instead of bulk Co layers in these $[Pt/Co]_n$ superlattices as $n \geqslant 2$. Meanwhile, magnetization is mainly determined by Co layers, especially as $n \leqslant 5$. In such a system where SOC and magnetism are separately determined by Pt and Co, respectively, spin polarization of the spin Hall angle (P_θ) can tend to be 0 as proposed in Ref. [32]. If so, Eq. (2) can thus be further reduced as $\eta = (1 - P_T/P)\theta_H S/(\mu_0 M_0)$. This means that a material-sensitive parameter (P_T/P) becomes measurable through the ANE. However, this measurement requires simultaneous determination of the Seebeck coeffcient and anomalous Nernst coefficient in the same well-defined temperature distribution, which cannot be completed in our setup and could be further investigated.

VIII. CONCLUSION

The ANE and AHE have been measured in $[Pt/Co]_n$ superlattices. Upon increasing the number of interfaces from 1 to 15, θ_H and ν_N increase simultaneously, by 430% and 350%, respectively, and meanwhile their S and M_0 vary in much smaller ranges. Furthermore, a linear scaling relation between θ_H and ν_N is revealed, with different slopes $d\theta_H/d\nu_N$ as $n \leqslant 5$ and $n \geqslant 5$, which is probably attributable to the increase in S and M_0. This linear relation observed in the same material system verifies a phenomenologic relation among η, θ_H, and S derived from linear response theory. The phenomenologic relation says that $\eta = (P - P_T)/(P + P_\theta)\theta_H S/(\mu_0 M_0)$. And it shows the following picture of the ANE: ∇T generates a pure spin current in a ferromagnetic conductor via the SDSE and the spin current is then transformed as a transverse charge current via the ISHE and, finally, leads to an observable anomalous Nernst voltage. Thus, a large ANE can be expected in some magnetically doped topological materials (such as Bi_2Se_3) where a large Seebeck coefficient and SOC strength coexist. This study not only shows an effective way to enhance the ANE but also experimentally demonstrates in the same material system an inherent relation between the ANE and the AHE and, further, proposes a way to determine the value of P_T/P in ferromagnetic conductors.

ACKNOWLEDGMENTS

This work was supported by the 863 Plan Project of Ministry of Science and Technology (MOST) (Grant No. 2014AA032904), the MOST National Key Scientific Instrument and Equipment Development Projects [Grant No. 2011YQ120053], the National Natural Science Foundation of China (NSFC) [Grant No. 11434014, 11222432, 11404382], the Strategic Priority Research Program (B) of the Chinese Academy of Sciences (CAS) [Grant No. XDB07030200] and Postdoctoral Science Foundation of China [Grant No. 2013M540154].

[1] K. Uchida, S. Takahashi, K. Harii, J. Ieda, W. Koshibae, K. Ando, S. Maekawa, and E. Saitoh, Nature **455**, 778 (2008).
[2] G. E. W. Bauer, E. Saitoh, and B. J. van Wees, Nat. Mater. **11**, 391 (2012).
[3] T. Kikkawa, K. Uchida, Y. Shiomi, Z. Qiu, D. Hou, D. Tian, H. Nakayama, X. F. Jin, and E. Saitoh, Phys. Rev. Lett. **110**, 067207 (2013).
[4] D. Qu, S. Y. Huang, J. Hu, R. Wu, and C. L. Chien, Phys. Rev. Lett. **110**, 067206 (2013).
[5] M. Schmid, S. Srichandan, D. Meier, T. Kuschel, J. M. Schmalhorst, M. Vogel, G. Reiss, C. Strunk, and C. H. Back, Phys. Rev. Lett. **111**, 187201 (2013).
[6] S. Y. Huang, W. G. Wang, S. F. Lee, J. Kwo, and C. L. Chien, Phys. Rev. Lett. **107**, 216604 (2011).
[7] S. Y. Huang, X. Fan, D. Qu, Y. P. Chen, W. G. Wang, J. Wu, T. Y. Chen, J. Q. Xiao, and C. L. Chien, Phys. Rev. Lett. **109**, 107204 (2012).
[8] H. Wu, C. H. Wan, Z. H. Yuan, X. Zhang, J. Jiang, Q. T. Zhang, Z. C. Wen, and X. F. Han, Phys. Rev. B **92**, 054404 (2015).
[9] C. M. Jaworski, J. Yang, S. Mack, D. D. Awschalom, J. P. Heremans, and R. C. Myers, Nat. Mater. **9**, 898 (2010).
[10] H. Jin, Z. Yang, R. C. Myers, and J. P. Heremans, Solid State Commun. **198**, 40 (2014).

[11] K. Uchida, J. Xiao, H. Adachi, J. Ohe, S. Takahashi, J. Ieda, T. Ota, Y. Kajiwara, H. Umezawa, H. Kawai, G. E. Bauer, S. Maekawa, and E. Saitoh, Nat. Mater. **9**, 894 (2010).
[12] K. Uchida, H. Adachi, T. Ota, H. Nakayama, S. Maekawa, and E. Saitoh, Appl. Phys. Lett. **97**, 172505 (2010).
[13] M. Walter, J. Walowski, V. Zbarsky, M. Munzenberg, M. Schafers, D. Ebke, G. Reiss, A. Thomas, P. Peretzki, M. Seibt, J. S. Moodera, M. Czerner, M. Bachmann, and C. Heiliger, Nat. Mater. **10**, 742 (2011).
[14] A. Boehnke, M. Walter, N. Roschewsky, T. Eggebrecht, V. Drewello, K. Rott, M. Munzenberg, A. Thomas, and G. Reiss, Rev. Sci. Instrum. **84**, 063905 (2013).
[15] W. Lin, M. Hehn, L. Chaput, B. Negulescu, S. Andrieu, F. Montaigne, and S. Mangin, Nat. Commun. **3**, 744 (2012).
[16] A. Slachter, F. L. Bakker, J. P. Adam, and B. J. van Wees, Nat. Phys. **6**, 879 (2010).
[17] F. K. Dejene, J. Flipse, and B. J. van Wees, Phys. Rev. B **86**, 024436 (2012).
[18] X. M. Zhang, C. H. Wan, Z. H. Yuan, H. Wu, Q. T. Zhang, X. Zhang, J. Jiang, B. S. Tao, and X. F. Han, arXiv:1506.03698.
[19] L. Gravier, S. Serrano-Guisan, F. Reuse, and J. P. Ansermet, Phys. Rev. B **73**, 052410 (2006).
[20] J. Flipse, F. L. Bakker, A. Slachter, F. K. Dejene, and B. J. van Wees, Nature Nanotechnol. **7**, 166 (2012).
[21] R. Ramos, M. H. Aguirre, A. Anadon, J. Blasco, I. Lucas, K. I. Uchida, P. A. Algarabel, L. Morellon, E. Saitoh, and M. R. Ibarra, Phys. Rev. B **90**, 054422 (2014).
[22] Y. Pu, D. Chiba, F. Matsukura, H. Ohno, and J. Shi, Phys. Rev. Lett. **101**, 117208 (2008).
[23] K. Hasegawa, M. Mizuguchi, Y. Sakuraba, T. Kamada, T. Kojima, T. Kubota, S. Mizukami, T. Miyazaki, and K. Takanashi, Appl. Phys. Lett. **106**, 252405 (2015).
[24] K. I. Uchida, T. Kikkawa, T. Seki, T. Oyake, J. Shiomi, Z. Qiu, K. Takanashi, and E. Saitoh, Phys. Rev. B **92**, 094414 (2015).
[25] A. D. Avery, S. J. Mason, D. Bassett, D. Wesenberg, and B. L. Zink, Phys. Rev. B **92**, 214410 (2015).
[26] W. M. Haynes (ed.), *CRC Handbook of Chemistry and Physics*, 92nd ed. (CRC Press, Boca Raton, FL, 2011).
[27] C. L. Canedy, X. W. Li, and G. Xiao, Phys. Rev. B **62**, 508 (2000).
[28] J. Zhao, Y. J. Wang, X. F. Han, S. Zhang, and X. H. Ma, Phys. Rev. B **81**, 172404 (2010).
[29] N. Nagaosa, J. Sinova, S. Onoda, A. H. MacDonald, and N. P. Ong, Rev. Mod. Phys. **82**, 1539 (2010).
[30] B. F. Miao, S. Y. Huang, D. Qu, and C. L. Chien, Phys. Rev. Lett. **111**, 066602 (2013).
[31] J. Chang, R. Daou, C. Proust, D. LeBoeuf, N. Doiron-Leyraud, F. Laliberte, B. Pingault, B. J. Ramshaw, R. Liang, D. A. Bonn, W. N. Hardy, H. Takagi, A. B. Antunes, I. Sheikin, K. Behnia, and L. Taillefer, Phys. Rev. Lett. **104**, 057005 (2010).
[32] K. Tauber, A. Honemann, D. V. Fedorov, M. Gradhand, and I. Mertig, Phys. Rev. B **91**, 220404 (2015).
[33] P. Poulopoulos, M. Angelakeris, E. T. Papaioannou, N. K. Flevaris, D. Niarchos, M. Nyvlt, V. Prosser, S. Visnovsky, C. Mueller, P. Fumagalli, F. Wilhelm, and A. Rogalev, J. Appl. Phys. **94**, 7662 (2003).
[34] J. Geissler, E. Goering, M. Justen, F. Weigand, G. Schütz, J. Langer, D. Schmitz, H. Maletta, and R. Mattheis, Phys. Rev. B **65**, 020405(R) (2001).
[35] A. A. Rudnitski, *Thermoelectric Properties of the Noble Metals and Their Alloys* (Academy of Sciences of the USSR Press, Moscow, 1956) [in Russian].